Magnetic graphene/Ni-nano-crystal hybrid for small field magnetoresistive effect synthesized via…

Article *in* Journal of Materials Science Materials in Electronics · November 2017

CITATIONS
0

READS
23

27 authors, including:

S. Erfanifam

11 PUBLICATIONS **61** CITATIONS

SEE PROFILE

Maryam Bahreini

Shahid Beheshti University

18 PUBLICATIONS **59** CITATIONS

SEE PROFILE

Mojtaba Ranjbar

National University of Singapore

29 PUBLICATIONS **284** CITATIONS

SEE PROFILE

Johan Åkerman

University of Gothenburg

255 PUBLICATIONS **4,219** CITATIONS

SEE PROFILE

Magnetic graphene/Ni-nano-crystal hybrid for small field magnetoresistive effect synthesized via electrochemical exfoliation/deposition technique

Z. Sheykhifard[1], S. Majid Mohseni[1,*], B. Tork[1], M.R. Hajiali[2], L. Jamilpanah[1], B. Rahmati[1], F. Haddadi[1], M. Hamdi[1], S. Morteza Mohseni[1], M. Mohammadbeigi[1], A. Ghaderi[1], S. Erfanifam[1], M. Dashtdar[1], F. Feghhi[3], N. Ansari[3], S. Pakdel[4], M. Pourfath[4], A. Hosseinzadegan[5], M. Bahreini[5], S.H. Tavassoli[5], M. Ranjbar[6], S.A.H. Banouazizi[7], S. Chung[7,8], J. Akerman[7,8], N. Nikkam[9], A. Sohrabi[10,11], S. E. Roozmeh[2]

[1] *Faculty of Physics, Shahid Beheshti University, Evin, Tehran 19839, Iran*

[2]*Department of Physics, University of Kashan, 87317 Kashan, Iran*

[3]*Department f Physics, Alzahra University, Tehran 19938, Iran*

[4]*School of Electrical and Computer Engineering, University of Tehran, Tehran 14395-515, Iran*

[5]*Laser and Plasma Research Institute, Shahid Beheshti University, Evin, Tehran, 19839, Iran*

[6]*School of Electrical, Computer and Energy Engineering, Arizona State University, Tempe, Arizona 85287 1504, USA*

[7]*Materials and Nano Physics, School of ICT, KTH Royal Institute of Technology, Electrum 229, 164 40 Kista, Sweden*

[8] *Department of Physics, University of Gothenburg, Fysikgränd 3, 412 96 Gothenburg, Sweden*

[9] *Faculty of Life Sciences and Biotechnology, Shahid Beheshti University, Tehran 19839, Iran*

[10]*Fouman Faculty of Engineering, College of Engineering, University of Tehran, P.O. Box 43515-1155, Fouman, Iran*

[11] *RACED Advanced Technology Development, Tehran, Iran*

[*]*Corresponding author email address: m-mohseni@sbu.ac.ir, majidmohseni@gmail.com*

Keywords: graphene heterostructure, magnetoresistance, magnetization, nano-crystal, electrochemical, exfoliation

Abstract

Two-dimensional heterostructures of graphene (Gr) and metal/semiconducting elements convey new direction in electronic devices. They can be useful for spintronics because of small spin orbit interaction of Gr as a non-magnetic metal host with promising electrochemical stability. In this paper, we demonstrate one-step fabrication of magnetic Ni-particles entrapped within Gr-flakes based on simultaneous electrochemical exfoliation/deposition procedure by two-electrode system using platinum as the cathode electrode and a graphite foil as the anode electrode. The final product is an air stable hybrid element including Gr flakes hosting magnetic Ni-nano-crystals showing superparamagnetic-like response and room temperature giant magnetoresistance (GMR) effect at small magnetic field range. The GMR effect is originated from spin scattering through ferromagnetic/non-magnetic nature of Ni/Gr heterostructure and interpreted based on a phenomenological spin transport model. Our work benefits from XRD, XPS, Raman, TEM, FTIR and VSM measurements We addressed that how our results can be used for rapid manufacturing of magnetic Gr for low field magneto resistive elements and potential printed spintronic devices.

1 Introduction

Spintronics aims to utilize the spin degree of freedom of electrons for new forms of information storage, logic devices, sensors, etc [1]. Recently, this field circumvents challenges with new concepts regarding spin-dependent phenomena in new materials, e.g. graphene (Gr) [2–4], transition metals chalcogenides (TMDs) [5–7] and topological insulators [8–10], etc. Application of Gr in spintronics and magnetism is one of open horizons for future research [11–14] based on the weak spin-orbit interaction of Gr. It means that spin can transport for a long range of a few microns at room temperature as a potential spin current channel for magnetoresistive [2,15–17], magnonic elements [18–21] and additionally has shown application in gate-tunable carrier concentration and high electronic mobility devices [22,23]. For example, exceptional magnetic response is very recently seen in Gr being adjusted to NiFe magnetic metal for magnetoresistance (MR) effect with 100% spin filtration [24], and YIG magnetic insulator, as proximity induced magnetic effect [25,26].

Gr family provides a supportive planar structure to bind with nanoparticles (NPs) for multi-functional purposes [27–30]. Formation of assembly of magnetic NPs on Gr or Gr–oxide flake surface exhibits novel magnetic properties [17,31–36] with highly promising application for bio-

medicine [37,38], microwave absorption [39,40], sensors [41–43] and environment. Nevertheless, there are still open doors to invest fundamental studies on combination of magnetism and Gr for many practical applications especially toward making stable magnetic elements for printed spintronics. As the printed electronics with Gr has shown to be highly promising [44–46], however print technology for spintronics circuits requires electrical conductivity and large content of magnetic specimen, that cannot be achieved by only using materials highly dominated by magnetic NPs with small production yield, long synthesis time and costly. Additional issues such as agglomeration of magnetic NPs and their small conductivity are major drawbacks. To suggest alternative solution, Gr hosting magnetic elements fabricated based on electrochemical synthesis that we introduce here can convey new direction in this area.

Electrochemical exfoliation of graphite has found upsurge attention to be scalable for Gr production [47] in simple and ambient conditions [48]. Exfoliation based this method has shown high quality and gram quantity of Gr in short time within several minutes to few hours. That shows easily alteration of Gr functionality through variation of precursors, electrolytes and voltage for supercapacitors [49,50], battery [51] photodetectors [52], transparent electrodes [53], mechanical elements [54], etc.

Recently, exfoliation of graphite into Gr flakes [49] with controlled metal doping, electrochemically stable and alternative electrical conductive [55] have shown promising scientific impact. Fabrication of heterostructure of metal based elements with Gr can provide dimension/scale matched into all 2D heterostructures, instead of commonly used volume-shaped three dimensional NPs adjacent to Gr layers. For example, GMR effect was seen in magnetic NPs/Gr composite made by hydrothermal effect [56]. It was proved that Gr contribution as a shell around magnetic NP core can highly increase the GMR response. However, fabrication technique for such GMR materials is complex and requires high temperature and long synthesis process as Gr and materials for magnetic NPs should be individually prepared from the beginning and transferred to form of composite dominant with large volume of magnetic NPs. Nevertheless, heterostructure materials could potentially represent alternative GMR results based on dominant interface effects. Therefore, such hybrid heterostructures made of planar geometry of Gr and magnetic metals show potentially interesting media for spintronic applications [57]. Nonetheless, fabrication of GMR elements including Gr and magnetic metal is usually based on single common microelectronic device [24,58] with high risk of manufacturing, expense and reproducibility.

However, their manufacturing into other state of the art of elements, i.e. in form of powders or ink, could be potentially demanding for many applications.

In this work, for the first time we report the one-step electrochemical synthesis of heterostructures of magnetic nano-crystals of Ni compounds deposited within exfoliated Gr flakes in an aqueous solution of $NiCl_2$. TEM images show that Ni-based elements are formed as nano-plate crystals faced with Gr flakes. Samples show superparamagnetic response at room temperature. Such heterostructures show GMR effect at room temperature in small magnetic field interval. The GMR effect is interpreted based on phenomenological scattering model. Our fabrication method as well as final products convey a path for application of novel magnetic and metal based Gr materials for printed electronics of spintronic devices and useful composite/materials for other purposes requiring metal based Gr heterostructures.

2 Sample preparation and experimental methods

Electrochemical exfoliation of graphite was performed in a two-electrode system using platinum (0.5×10 cm^2) as the cathode electrode and a graphite foil (2×10 cm^2) as the anode electrode. The purity of used electrodes was higher than 99%.The distance between two electrodes was kept fix at 2.7 cm. The electrolyte was prepared by dissolving $NiCl_2.6H_2O$ powder (98.0% Merck) in water (concentration of 0.05 M and pH ~6.5−7.0). The voltage of 10 V was applied to provide expansion, exfoliation of graphite and deposition of Ni. During the whole process, to avoid accumulation of the product on cathode, the Pt electrode was washed every 20 min with HCl then water. Finally, the products collected using vacuum filtration and washed with water. The resulted product was dispersible for sonication in water (Fig. 1).

the mechanism of electrochemical exfoliation depicted is explained in Fig. 1. Firstly, by applying the voltage between electrodes, hydroxyl ions (OH^-) are produced in the cathode region and then accelerate towards the anode and hit the graphite surface. The collision of graphite with OH^- ions initially occurs at each side and grain boundaries (Fig. 1a). The oxidation at the edge side and grain boundaries leads to expansion of the graphite layers and Cl^- ions can penetrate through them and reduction of Cl^- ions produce Cl gas (Fig. 1b). The gas can exert excessive force to graphite layers which results in separation of the graphite layers [47,57] (Fig. 1c). In continue, Gr sheets distributed in the solution can trap Ni^{2+} ions (Fig. 1d). Since such sheets have been partially positive charged, and because of polarization of Gr in electric field they can accelerate towards the

negative electrode under electric field and create black composite on Pt electrode. As known the hydroxyl generation occurs at cathode by ionization of water as follows [60]:

$$2H_2O + 2e^- \rightarrow H_2 + 2OH^- \quad (1)$$

The OH^- generation together with other electrons and ions can form Ni and $Ni(OH)_2$ on Gr sheets. Based on all above process, we finally have Ni and $Ni(OH)_2$ deposited as crystalline layers on Gr flakes (Fig. 1e).

The final product in form of powder was pressed (under pressure of 5 MPa for 30 min) into pellets for MR measurements. Samples dimension were 6.5 mm (radius) and 1 mm (thickness), approximately. The MR was measured at room temperature using a standard two probe method. The Ni-Gr composite samples were characterized by X-ray diffraction (XRD, Cu Kα $\lambda = 0.154$ nm) radiation, Raman spectroscopy (RM N1-541, 532 nm laser beam), X-ray photoelectron spectroscopy (XPS, ESCA/AES, CHA, Specs model EA10 plus), Fourier transform infrared spectroscopy (FTIR, Bruker Tensor 27, resolution of 1 cm^{-1} in transmission mode), tunneling electron microscopy (TEM-Philips model CM120), vibrating sample magnetometer (VSM, Meghnatis Daghigh Kavir Co.) and dynamic light scattering (DLS, Malvern Instruments Ltd, Worcestershire).

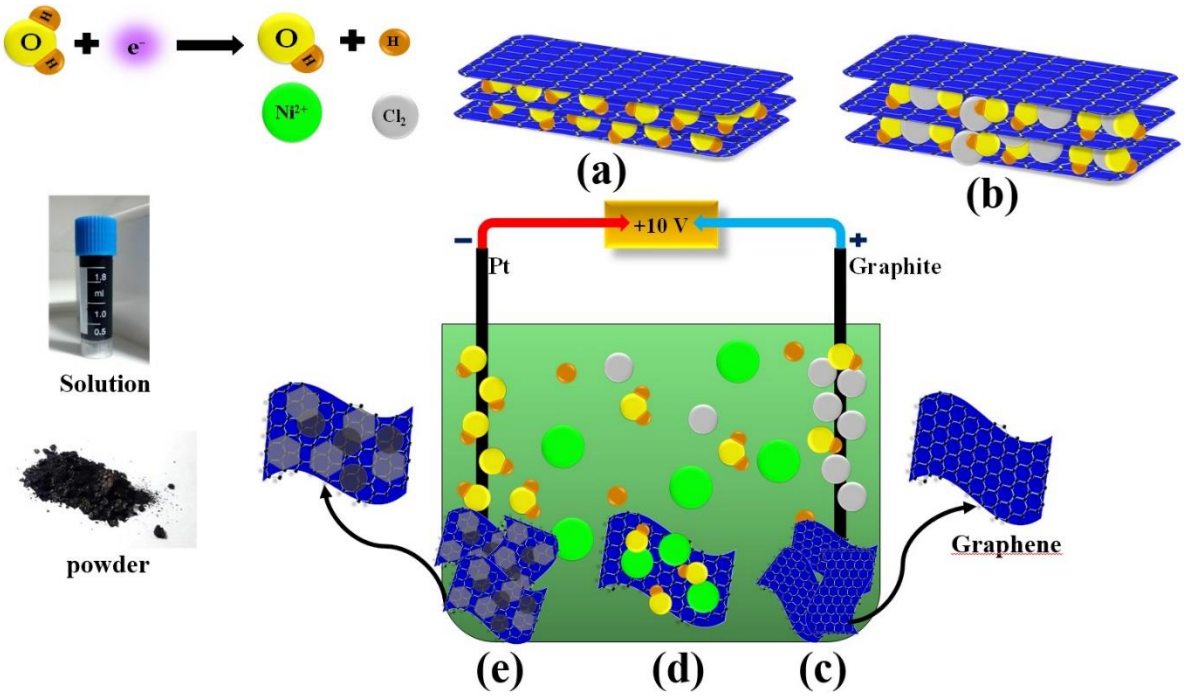

Fig. 1 Schematic illustration of the proposed mechanism for magnetic Gr production, **a** representation of OH^- ions between graphite sheets which increases the interlayer distance, **b** presence of the Cl^- ions between graphite sheets, **c** Exfoliated Gr sheets under pressure due to Cl gas, **d** trapping Ni ions by Gr flakes and their movement towards Pt electrode under electric field, **e** arrival of Gr and Ni ions to Pt and formation of Ni based elements. Gr-Ni heterostructure composites are dried and dispersed in water.

3 Results and discussion

Figure 2 displays the XRD pattern of Gr-Ni sample compared with graphite. As can be seen, the major diffraction peak of graphite at $2\theta = 26.31°$ indicates an interlayer d-spacing of 3.38 Å, while in the final sample the (002) diffraction peak is appeared at 26.16° with an interlayer d-spacing of 3.40 Å. The slightly smaller 2θ angle of exfoliated Gr with large d-spacing compared to that for graphite suggests the Gr-Ni contains only a small amount of functional groups [49] In addition, we speculate that as Ni crystals are entrapped within Gr flakes with dominated intensity in XRD pattern, any signature of Gr in XRD is undetectable [54]. There are some diffraction peaks that belong to $Ni(OH)_2$. Those peaks at $2\theta = 18.76°$, $2\theta = 32.80°$, $2\theta = 38.19°$, $2\theta = 62.32°$, $2\theta = 69.28°$ and $2\theta = 72.55°$ belong to (001), (100), (101), (111), (200) and (201) planes of the β-phase (JCPDS No: 001-1047) [61]. Peaks at $2\theta = 44.1°$ and 51.58° correspond to (111) and (200) planes of face centered cubic (fcc) Ni with lattice constant of 3.54 Å (JCPDS No: 001-1258). Peaks at $2\theta = 58.72°$ is related to (012) plane of hexagonal structure of Ni (JCPDS No: 045-1027). The monoclinic

crystalline $NiCl(H_2O)_6$ phase has two main peaks at the diffraction angles of 15.88◦ and 64.49◦ (JCPDS No: 073-0496) which are related to the initial salt used in experiment. The average crystal size of deposited Ni and $Ni(OH)_2$ nano-crystals calculated based on Scherrer equation were found at 43 and 32 nm, respectively, values are close to those observed in TEM images that will be explained later.

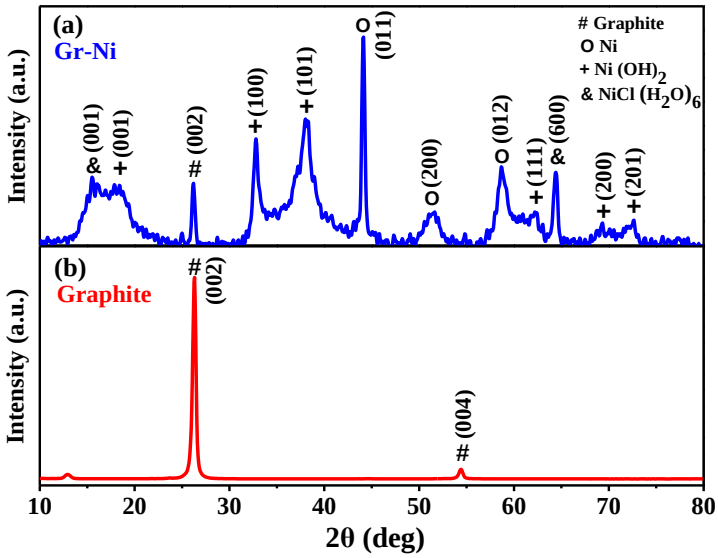

Fig. 2 XRD results of **a** Gr-Ni sample and **b** graphite foil.

High-resolution XPS spectra of Gr-Ni structures are shown in Fig. 3 a, b. The C 1s (Fig. 3a) and Ni 2p (Fig. 3b) peaks were decomposed into multi-peaks analyzing with distribution of C–C/C–O/C=O and Ni–O/ Ni–OH bonds [62]. Results of XPS measurement are very briefly discussed here and we leave detail analyses of this measurement in the supplementary note. The peak data are presented in Table 1. Most of peaks related to Ni 2p show presence of $Ni(OH)_2$ and Ni-oxides and no Ni, contrary to those seen in XRD measurements. The former statement reconfirms the presence of Ni compounds at surface of layers which is expected as the XPS is able to probe the surface only. Therefore, these analyses together with those peaks in XRD potentially suggest that Ni-crystals are sandwiched between flakes and other crystals which remain electrochemically stable, as reconfirmed by magnetization measurements. The Raman scattering is a well-accepted characterization method for evaluating the structure of initial used graphite foil and Gr-Ni structures. The Raman spectra clearly show peaks at the wave numbers of 1583, 1358 and 2705

cm^{-1}, indicating the presence of the G peak, D peak and 2D band characteristics of Gr, respectively (Fig. S2), hence the incorporation of Gr in the Gr-Ni composites. Further details of XPS measurement results together with FTIR also Raman measurements are addressed in supplementary details. They show decreasing layer number of initial graphite foils and sign of presence of Ni-based layers in the final sample.

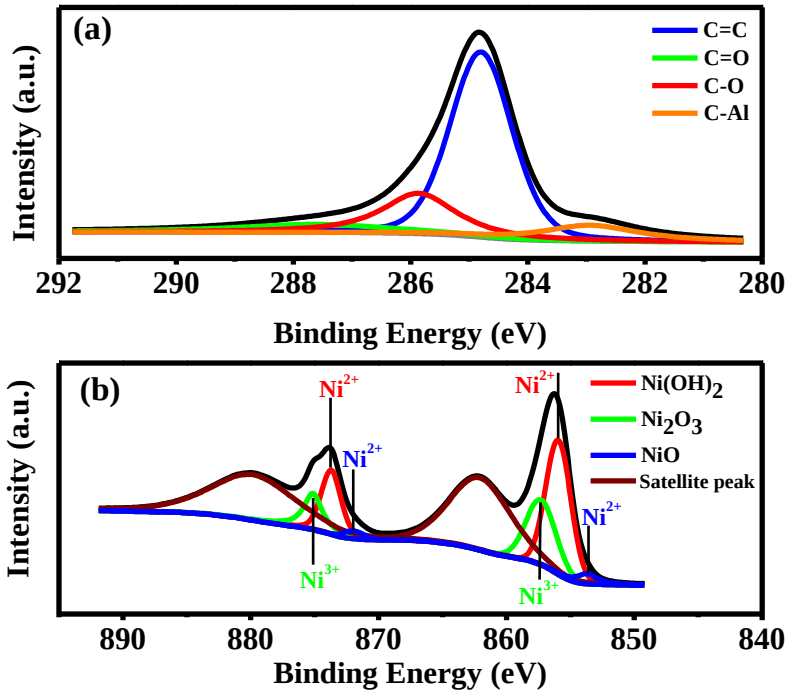

Fig. 3 XPS of Gr-Ni sample **a** C1s core-level and **b** Ni 2p core-level.

Table 1 Peak positions and FWHM values from high-resolution XPS spectra of C 1s and Ni 2p core level of Gr-Ni sample.

	C1s (C–Al)	C1s (C=C)	C1s (C–O)	C1s (C=O)	$Ni2p_{3/2}(Ni^{2+})$	$Ni2p_{3/2}(Ni^{3+})$	$Ni2p_{1/2}(Ni^{2+})$	$Ni2p_{1/2}(Ni^{3+})$
B.E. (eV)	282.5	284.8	285.9	278.6	855.9 853.7	857.4	873.6 871.9	875.1
FWHM (eV)	2	1.3	1.7	4.1	2.3 1.9	2.7	1.8 1.9	1.7

TEM image of Gr-Ni samples shown in Fig. 4a represents crumpled Gr layers decorated with particle-like elements. There are spherical and hexagonal structures and other crystal geometries which some are rolled up (shown by arrows) are presumed to be related mainly to Ni and Ni-based nano-crystals (Fig. 4b). Also XRD results prove that fcc and hexagonal structures of this Ni based

elements are formed. Comparing all features dictates small thickness of such crystal, as they look to have thin planar geometry. The nano-crystals (Ni, $Ni(OH)_2$, Ni-oxides) are randomly distributed on Gr sheets which are supposed to be the reason of their superparamagnetic like response. The size of nano-crystal is obtained by TEM and XRD patterns in range of 30-40 nm. The brightness of Gr sheets appearing in these images shows their small thickness. The image in Fig. 4a shows micron boundary size formation of Gr sheets which is in agreement with DLS result that determined to be about 1.2 μm in the solution. We can conclude that our one-step fabrication method, reported for the first time, is capable of yielding Gr/(magnetic nano-crystal) heterostructures.

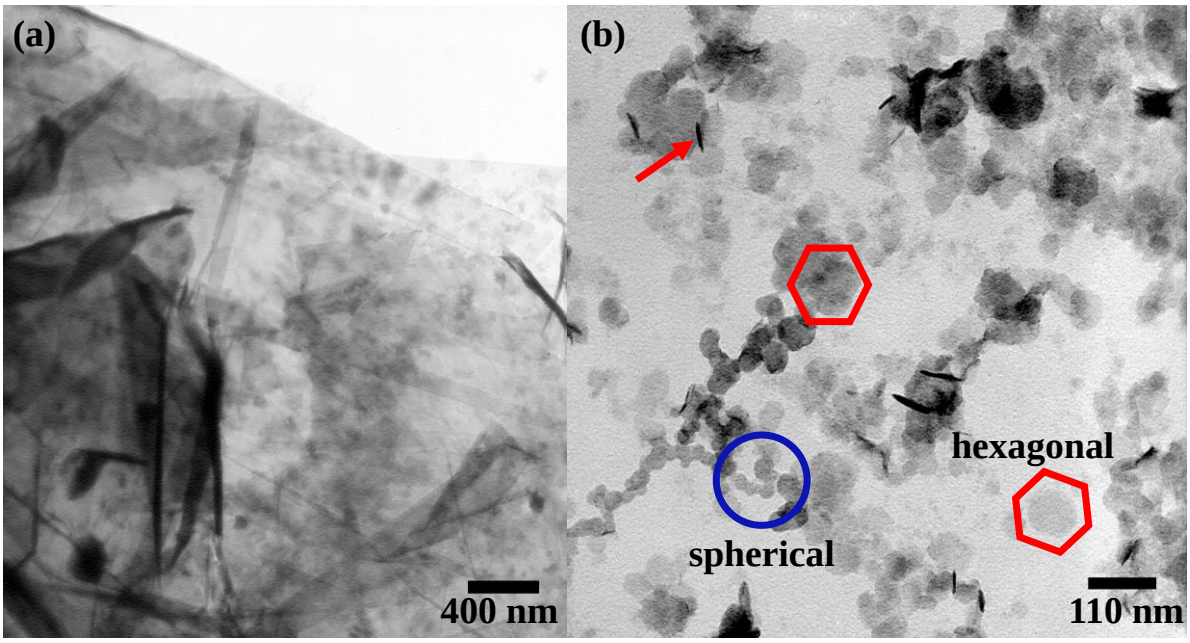

Fig. 4 TEM images of **a** micron boundary size of Gr sheets and **b** different geometry of Gr-Ni samples.

As depicted in Fig. 5, we performed magnetic measurements of the Gr–Ni composite by VSM at room temperatures. Those Ni-crystals distributed between Gr flakes have small interaction and hence sample shows superparamagnetic-like response, similar to many reports [63,64] which have been reported superparamagnetic behavior in nanoparticles with sizes bellow 100 nm. The magnetic moment of approximately 1 emu/g, not though large, confirms contribution of Ni content as none of Ni-oxide and Ni-hydroxide compounds have net magnetic moment at room temperature. Interestingly, the magnetization changes a little for the same sample measured after one year

dictating electrochemical stability of this structure after leaving in air for a long time. As depicted in inset, there are no indeed changes in coercive field in a small field interval.

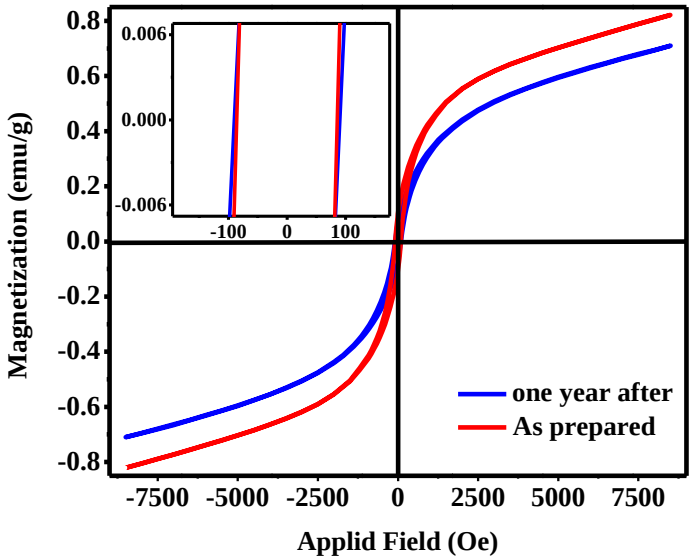

Fig.5 Room temperature VSM magnetization of Gr-Ni samples measured immediately and one year after. The inset shows the low-field area.

These Gr-Ni crystalline composites are more similar to granular ferromagnetic (FM) metal/ nonmagnetic (NM) metal complexes that show granular GMR [65]. Positive linear magnetoresistance (LMR) effect was seen earlier in Carbon (graphite) based Ni_x-C_{1-x} granular composites [66] at large fields up to 5T at room temperatures. Here, Gr flakes contain FM Ni-based nano-crystal 2D-plates distributed between Gr sheets as NM spacer, as represented schematically in Fig. 6a. It is expected to observe negative GMR effect, similar to that recently seen in single device [24] and contrary to the observed LMR in Ni_x-C_{1-x}. For GMR measurement, 2-point contacts placed on Gr-Ni palette sample and magnetic field applied between ±1.2 kOe by electromagnet. Results of GMR measurement is shown in Fig. 6b, represents absolute value of GMR ratio to be ~0.5% against magnetic field. Here, similar to what is shown in Fig. 6a, resistance is high at zero field originated from high spin scattering rate through magnetic cites as they are randomly magnetized. Resistance decreases with increasing applied magnetic field as magnetic cite are being ferromagnetically aligned and spin scattering rare decreases. We believe that our

result can address the applicability of using electrochemical exfoliation-deposition method for developing magnetic graphene based materials in spintronic elements.

To provide insight to the behavior of GMR of the Gr-Ni sample, we describe the magnetic properties of the system at first. From XRD and TEM results, Ni-crystals are nanometer in size and they are single magnetic domain planar particles. For simplicity, we suppose that the coercivity is negligible and there is no magnetic coupling (both exchange and dipolar) between magnetic particles. The GMR in such systems is an even function of net magnetization $(\frac{\mathrm{M}}{\mathrm{M_s}})$ and the GMR ratio is given by [65]

$$\left(\frac{\Delta\rho}{\rho}\right) = \frac{\rho(\mathrm{H}) - \rho_{max}}{\rho_{max}} = -\mathrm{A\ F}\left(\frac{\mathrm{M}}{\mathrm{M_s}}\right) \tag{2}$$

Where $\rho(\mathrm{H})$ is the resistance of sample at a given field strength H and ρ_{max} is the maximum resistivity of sample, A is the magnitude of GMR, F(x) is an even function of x. Based on the first order approximation [65], $\mathrm{F} = (\mathrm{M}/\mathrm{M_s})^2$. Figure 6c shows the GMR ratio versus net magnetization of the system. Filled black circles are experimental data extracted from GMR and magnetization curves, for a given magnetic field. The GMR ratio is obtained by the magnitude of resistivity at remanence. Red solid line is the fit of experimental data by equation (2). An excellent consistency between experimental data and fitted curve occurs for A=0.05495 which leads to a MR% value of 0.5%. For a comparison, one can define a MR rate as

$$r = \frac{MR\%}{\Delta H} = \frac{MR\%}{H_{max}} \tag{3}$$

in which, $MR\%$ is the magnetoresistance ratio defined by Eq. 2 and $\Delta H = H_{max}$ is the maximum field applied in the measurement. For our Gr-Ni crystalline composites we find a value of r =4.1 which is better than $r = 2$ for LMR reported on Ni_x-C_{1-x} [66] at room temperature.

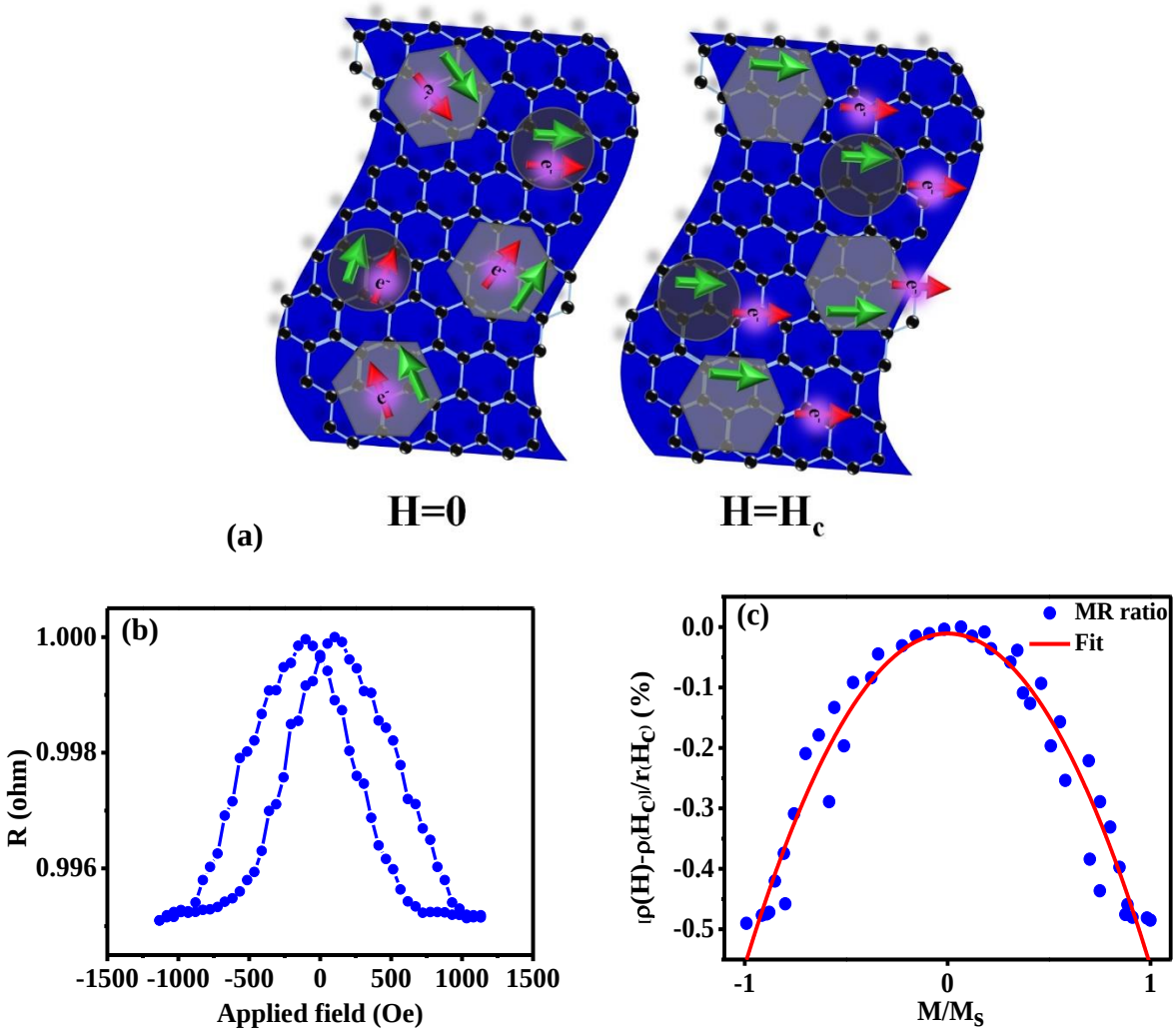

Fig. 6 a Schematic illustration of magnetic elements on Gr sheets, and spin scattering through the system with or without applied magnetic field, **b** GMR measurement against applied magnetic field and **c** GMR versus magnetization.

4 Conclusion

In conclusion, we demonstrate one step facile fabrication of Gr flakes decorated in face with magnetic nano-crystals in heterostructure form. FTIR shows a number of oxygen functionalities and this may be because of the residual functional groups in Gr. The Raman scattering address lower number of layers for obtained samples rather than graphite foil and the peak located at (500 cm^{-1}) in Gr-Ni structures is attributed to $Ni(OH)_2$. Our final products, as seen in TEM images, as in face to face stacking of Ni-metal/hydroxide elements with Gr sheets can be potentially useful for many applications. Potential ability of such unique hybrid stack is explored as heterostructure

of FM/NM design for GMR element. The statement of randomly magnetized nano-crystals as spin scatterers at zero field changes to that of well-defined scattering mechanism at higher field within Gr flakes that interprets the GMR effect. We examined our final materials one year after their production and have not seen significant changes in their magnetization, revealed by VSM, dictating that they are highly stable materials for application in normal environment. Such air stable material is highly promising for application of inkjet printed spintronic elements, and other state of the art of Gr-based metal/semiconductor devices for electronics, energy harvesting and Gr-metal-decorated wiring devices.

Acknowledgments

S.M.M. acknowledges support from Iran Science Elites Federation (ISEF), Iran's Cognitive Sciences and Technologies Council under contract number 2714, Iran National Science Foundation (INSF), Iran Nanotechnology Initiative Council and Iran's National Elites Foundation (INEF). We thank Prof. Omar Yaghi for his useful comments on the manuscript.

References

1. I. Žutić, J. Fabian, and S. Das Sarma, Rev Mod Phys **76**, 323 (2004).

2. N. Tombros, C. Jozsa, M. Popinciuc, H. T. Jonkman, and B. J. van Wees, Nature **448**, 571 (2007).

3. D. Pesin and A. H. MacDonald, Nat Mater **11**, 409 (2012).

4. W. Han, R. K. Kawakami, M. Gmitra, and J. Fabian, Nat Nanotechnol **9**, 794 (2014).

5. W. Zhang, J. Sklenar, B. Hsu, W. Jiang, M. B. Jungfleisch, J. Xiao, F. Y. Fradin, Y. Liu, J. E. Pearson, J. B. Ketterson, Z. Yang, and A. Hoffmann, APL Mater **4**, 32302 (2016).

6. Z. Wang, D.-K. Ki, J. Y. Khoo, D. Mauro, H. Berger, L. S. Levitov, and A. F. Morpurgo, Phys Rev X **6**, 41020 (2016).

7. Q. Shao, G. Yu, Y.-W. Lan, Y. Shi, M.-Y. Li, C. Zheng, X. Zhu, L.-J. Li, P. K. Amiri, and K. L. Wang, Nano Lett **16**, 7514 (2016).

8. A. R. Mellnik, J. S. Lee, A. Richardella, J. L. Grab, P. J. Mintun, M. H. Fischer, A. Vaezi, A. Manchon, E.-A. Kim, N. Samarth, and D. C. Ralph, Nature **511**, 449 (2014).

9. Y. Fan, P. Upadhyaya, X. Kou, M. Lang, S. Takei, Z. Wang, J. Tang, L. He, L. Chang, M. Montazeri, G. Yu, W. Jiang, T. Nie, R. N. Schwartz, Y. Tserkovnyak, and K. L. Wang, Nat Mater **13**, 699 (2014).

10. Y. Fan, X. Kou, P. Upadhyaya, Q. Shao, L. Pan, M. Lang, X. Che, J. Tang, M. Montazeri, K. Murata, L.-T. Chang, M. Akyol, G. Yu, T. Nie, K. L. Wong, J. Liu, Y. Wang, Y. Tserkovnyak, and K. L. Wang, Nat Nanotechnol **11**, 352 (2016).

11. S. Roche, J. Åkerman, B. Beschoten, J.-C. Charlier, M. Chshiev, S. Prasad Dash, B. Dlubak, J. Fabian, A. Fert, M. Guimarães, F. Guinea, I. Grigorieva, C. Schönenberger, P. Seneor, C. Stampfer, S. O. Valenzuela, X. Waintal, and B. van Wees, 2D Mater **2**, 30202 (2015).

12. F. Volmer, M. Drögeler, T. Pohlmann, G. Güntherodt, C. Stampfer, and B. Beschoten, 2D Mater **2**, 24001 (2015).

13. J. Balakrishnan, G. Kok Wai Koon, M. Jaiswal, A. H. Castro Neto, and B. Özyilmaz, Nat Phys **9**, 284 (2013).

14. J. Balakrishnan, G. K. W. Koon, A. Avsar, Y. Ho, J. H. Lee, M. Jaiswal, S.-J. Baeck, J.-H. Ahn, A. Ferreira, M. a Cazalilla, A. H. Castro Neto, and B. Özyilmaz, Nat Commun **5**, 4748 (2014).

15. W. Han, K. Pi, K. M. McCreary, Y. Li, J. J. I. Wong, A. G. Swartz, and R. K. Kawakami, Phys Rev Lett **105**, 167202 (2010).

16. T.-Y. Yang, J. Balakrishnan, F. Volmer, A. Avsar, M. Jaiswal, J. Samm, S. R. Ali, A. Pachoud, M. Zeng, M. Popinciuc, G. Güntherodt, B. Beschoten, and B. Özyilmaz, Phys Rev Lett **107**, 47206 (2011).

17. N. Naseri, S. Solaymani, A. Ghaderi, M. Bramowicz, S. Kulesza, Ş. Ţălu, M. Pourreza, and S. Ghasemi, RSC Adv **7**, 12923 (2017).

18. B. Raes, J. E. Scheerder, M. V. Costache, F. Bonell, J. F. Sierra, J. Cuppens, J. Van de Vondel, and S. O. Valenzuela, Nat Commun **7**, 11444 (2016).

19. Z. Wang, D.-K. Ki, H. Chen, H. Berger, A. H. MacDonald, and A. F. Morpurgo, Nat Commun **6**, 8339 (2015).

20. M. Ranjbar, R. Sbiaa, S. M. Mohseni, M. Rahimabady, and S. N. Piramanayagam, Mater Today **19**, 368 (2016).

21. C. Cervetti, A. Rettori, M. G. Pini, A. Cornia, A. Repollés, F. Luis, M. Dressel, S. Rauschenbach, K. Kern, M. Burghard, and L. Bogani, Nat Mater **15**, 164 (2016).

22. A. H. Castro Neto, F. Guinea, N. M. R. Peres, K. S. Novoselov, and A. K. Geim, Rev Mod Phys **81**, 109 (2009).

23. F. Molitor, J. Güttinger, C. Stampfer, S. Dröscher, A. Jacobsen, T. Ihn, and K. Ensslin, J Phys Condens Matter **23**, 243201 (2011).

24. E. D. Cobas, O. M. J. van 't Erve, S.-F. Cheng, J. C. Culbertson, G. G. Jernigan, K. Bussman, and B. T. Jonker, ACS Nano **10**, 10357 (2016).

25. Z. Wang, C. Tang, R. Sachs, Y. Barlas, and J. Shi, Phys Rev Lett **114**, 16603 (2014).

26. J. C. Leutenantsmeyer, A. A. Kaverzin, M. Wojtaszek, and B. J. van Wees, 2D Mater **4**, 14001 (2016).

27. V. Dalouji, S. M. Elahi, S. Solaymani, and A. Ghaderi, Eur Phys J Plus **131**, (2016).

28. T. Ghodselahi, S. Solaymani, M. Akbarzadeh Pasha, and M. a. Vesaghi, Eur Phys J D **66**, 299 (2012).

29. Ş. Ţălu, S. Solaymani, M. Bramowicz, N. Naseri, S. Kulesza, and A. Ghaderi, RSC Adv **6**, 27228 (2016).

30. Ş. Ţălu, Napoca Star Publishing House, Cluj-Napoca, Romania, (2015).

31. B. Li, H. Cao, J. Yin, Y. A. Wu, and J. H. Warner, J Mater Chem **22**, 1876 (2012).

32. J. Tuček, Z. Sofer, D. Bouša, M. Pumera, K. Holá, A. Malá, K. Poláková, M. Havrdová, K. Čépe, O. Tomanec, and R. Zbořil, Nat Commun **7**, 12879 (2016).

33. V. Dalouji, S. Elahi, S. Solaymani, A. Ghaderi, and H. Elahi, Appl Phys A Mater Sci Process **122**, 1 (2016).

34. V. Dalouji, S. M. Elahi, A. Ghaderi, and S. Solaymani, Chinese Phys Lett **33**, 3 (2016).

35. Ş. Ţălu, M. Bramowicz, S. Kulesza, V. Dalouji, S. Solaymani, and S. Valedbagi, Microsc Res Tech **79**, 1208 (2016).

36. G. Zhu, Y. Liu, Z. Xu, T. Jiang, C. Zhang, X. Li, and G. Qi, Chemphyschem **11**, 2432 (2010).

37. W. J. Stark, Angew Chem Int Ed Engl **50**, 1242 (2011).

38. Z. Li, L. Wei, M. Y. Gao, and H. Lei, Adv Mater **17**, 1001 (2005).

39. H.-L. Xu, H. Bi, and R.-B. Yang, J Appl Phys **111**, 07A522 (2012).

40. M. Zong, Y. Huang, Y. Zhao, X. Sun, C. Qu, D. Luo, and J. Zheng, RSC Adv **3**, 23638 (2013).

41. H. Teymourian, A. Salimi, and S. Khezrian, Biosens Bioelectron **49**, 1 (2013).

42. A. Ambrosi, C. K. Chua, A. Bonanni, and M. Pumera, Chem Rev **114**, 7150 (2014).

43. Y. He, Q. Sheng, J. Zheng, M. Wang, and B. Liu, Electrochim Acta **56**, 2471 (2011).

44. A. G. Kelly, T. Hallam, C. Backes, A. Harvey, A. S. Esmaeily, I. Godwin, J. Coelho, V. Nicolosi, J. Lauth, A. Kulkarni, S. Kinge, L. D. A. Siebbeles, G. S. Duesberg, and J. N. Coleman, Science (80-) **356**, 69 (2017).

45. D. Makarov, D. Karnaushenko, and O. G. Schmidt, Chemphyschem **14**, 1771 (2013).

46. D. McManus, S. Vranic, F. Withers, V. Sanchez-Romaguera, M. Macucci, H. Yang, R. Sorrentino, K. Parvez, S.-K. Son, G. Iannaccone, K. Kostarelos, G. Fiori, and C. Casiraghi, Nat Nanotechnol **12**, 343 (2017).

47. C. T. J. Low, F. C. Walsh, M. H. Chakrabarti, M. A. Hashim, and M. A. Hussain, Carbon N Y **54**, 1 (2013).

48. A. M. Abdelkader, A. J. Cooper, R. A. W. Dryfe, and I. A. Kinloch, Nanoscale **7**, 6944 (2015).

49. K. Parvez, Z. Wu, R. Li, X. Liu, R. Graf, X. Feng, and K. Müllen, J Am Chem Soc **136**, 6083 (2014).

50. Z.-S. Wu, K. Parvez, S. Li, S. Yang, Z. Liu, S. Liu, X. Feng, and K. Müllen, Adv Mater **27**, 4054 (2015).

51. W. Wei, G. Wang, S. Yang, X. Feng, and K. Müllen, J Am Chem Soc **137**, 5576 (2015).

52. Z. Liu, K. Parvez, R. Li, R. Dong, X. Feng, and K. Müllen, Adv Mater **27**, 669 (2015).

53. Y. Xu and J. Liu, Small **12**, 1400 (2016).

54. Z. Ren, N. Meng, K. Shehzad, Y. Xu, S. Qu, B. Yu, and J. K. Luo, Nanotechnology **26**, 65706 (2015).

55. N. Chen, X. Huang, and L. Qu, Phys. Chem. Chem. Phys. **17**, 32077 (2015).

56. G. Abellán, H. Prima-García, and E. Coronado, J Mater Chem C **4**, 2252 (2016).

57. B. Dlubak, M. B. Martin, R. S. Weatherup, H. Yang, C. Deranlot, R. Blume, R. Schloegl, A. Fert, A. Anane, S. Hofmann, P. Seneor, and J. Robertson, ACS Nano **6**, 10930 (2012).

58. P. Leclair, J. K. Ha, H. J. M. Swagten, J. T. Kohlhepp, C. H. Van De Vin, and W. J. M. De Jonge, Appl Phys Lett **80**, 625 (2002).

59. K. Parvez, R. Li, S. R. Puniredd, Y. Hernandez, F. Hinkel, S. Wang, X. Feng, and K. Mullen, ACS Nano **7**, 3598 (2013).

60. M. Aghazadeh, A. N. Golikand, and M. Ghaemi, Int J Hydrogen Energy **36**, 8674 (2011).

61. D. S. Hall, D. J. Lockwood, C. Bock, and B. R. MacDougall, Proc Math Phys Eng Sci **471**, 20140792 (2015).

62. J. Fan, G. Li, D. Luo, C. Fu, Q. Li, J. Zheng, and L. Li, Electrochim Acta **173**, 7 (2015).

63. F. J. Owens and V. Stepanov, J Exp Nanosci **3**, 41 (2008).

64. C. Chouly, D. Pouliquen, I. Lucet, J. J. Jeune, and P. Jallet, J Microencapsul **13**, 245 (1996).

65. C. L. Chien, J. Q. Xiao, and J. S. Jiang, J Appl Phys **73**, 5309 (1993).

66. Q. Z. Xue and X. Zhang, Phys Lett A **313**, 461 (2003).